Chemical and Process Engineering 2021, 42 (4), 391–410
DOI: 10.24425/cpe.2021.138937

Energetic efficiency of mixing in a periodically reoriented Dean flow

Antoni Rożeń*, Janusz Kopytowski

Warsaw University of Technology, Faculty of Chemical and Process Engineering,
Waryńskiego 1, 00-645 Warszawa, Poland

In memory of Professor Jerzy Bałdyga

The energetic efficiency of mixing is studied numerically in a continuous flow mixer constructed from a sequence of alternately twisted pipe bends. Counter-rotating vortices present in the curved channels and known as Dean vortices narrow the distribution of the residence time of fluid elements and accelerate the generation of a new material surface without obstructing the main flow and increasing the risk of fouling or flow stoppage. Cyclic twisting of the pipe curvature allows for quick reorientation of Dean vortices. The reorientation induces chaotic advection in a stable three-dimensional flow and speeds up mixing. The effect of computational domain discretisation for the low and medium Reynolds numbers ($20 < \mathrm{Re} < 2000$) on the head loss, primary and secondary flow, residence time distribution, and the energetic efficiency of generation of the inter material surface is determined. The energetic efficiency is calculated in the time space, a standard approach in modelling reactive micromixing, and at the reactor exit. The maximum energetic efficiency is determined for $\mathrm{Re} \approx 600 \div 700$. It is also found that the initial orientation of the material surface to the pipe curvature has a significant impact on the energetic efficiency of mixing.

Keywords: computational fluid dynamics, laminar flow, chaotic advection, curvilinear pipes, time analysis

1. INTRODUCTION

Tubular mixers and chemical reactors, separation units and mass exchange systems built from curvilinear ducts have found a wide application in industrial practice. Similarly, as static, injector or impinging jet mixers or reactors, curved tube systems have no moving parts and operate in the laminar, mixed and turbulent flow regimes. Tubular mixers with curvilinear geometry are additionally characterised by low pumping costs and a low risk of fouling or an accidental flow stoppage due to the lack of tube inserts promoting mixing. These mixers also have a large heat and mass transfer surface per an active system volume and demonstrate a limited possibility of mechanical and thermal degradation of a processed material due to moderate levels of shear rate (Vashisth et al., 2008). Counter-rotating vortices, known as Dean vortices, are characteristic of the laminar and mixed flow in the curved ducts (Dean, 1928). The actual strength and pattern of the secondary flow depend on the channel curvature, the shape of the channel cross-section and,

* Corresponding author, e-mail: antoni.rozen@pw.edu.pl

as shown in Fig. 1, on the Reynolds number. Dean vortices are created by an imbalance between inertia and viscous forces present in the curvilinear flow, which generates the streamwise vorticity of the flow field. These flow structures carry high energy fluid elements from the channel centre to the channel walls, increasing friction losses while accelerating heat and mass transport. For example, Manlapaz and Churchil (1981) demonstrated that heat transfer coefficients are higher in the curved channel than in straight one in the same flow conditions. Saxena and Nigam (1983) proved that Dean flow reduces longitudinal dispersion of fluid components, while Moulin et al. (1996) found that Dean vortices improve oxygen transport towards the channel walls.

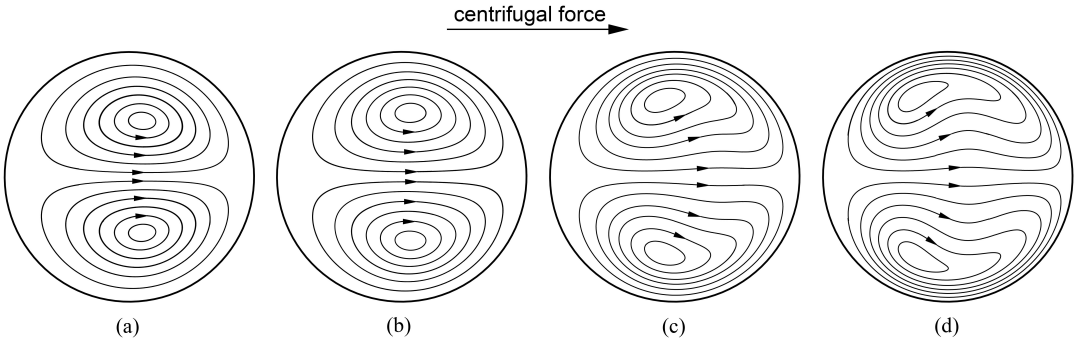

Fig. 1. Dean vortices formed in the toroidal channel of the curvature ratio $\delta = 0.08$: (a) Re = 100, (b) Re = 200, (c) Re = 500, (d) Re = 1000

However, when fluid particles become trapped inside Dean vortices, further improvement of mixing requires switching the flow structure from a regular to chaotic one. It can be done by having Dean vortices periodically destroyed and formed again and rotated or reshaped if possible. According to Aref (1984), the chaotic Lagrangian trajectories of fluid elements can be generated in a steady, three-dimensional flow which is integrable in the Eulerian sense by periodically reorienting the main flow. Indeed, if the tube mixer is assembled from short segments of curved pipes twisted alternately, deterministic chaos appears in the system, as demonstrated by Jones et al. (1989) and Sawyers et al. (1996). Chaotic advection intensifies mixing in a macroscale by narrowing the residence time distribution of fluid elements (Castelain et al., 2000). It also may accelerate mixing in a microscale by enhancing the stretching of material lines (Yamagishi et al., 2007) or by accelerating molecular diffusion of substrates towards the reaction zone (Boesinger et al., 2005; Rożeń and Kopytowski, 2020).

Mixing can be further improved either by flow destabilisation leading to the formation of an additional pair of small counter-rotating vortices (Nandacumar and Masliyah, 1982) or by switching to the transient/turbulent flow regime (Re $\gg$ 1000). However, the latter option may not be optimal when processing highly viscous liquids or materials susceptible to mechanical and thermal degradation caused by high shear rates.

Mixing in the curved tube systems is studied by passive as well as by reactive tracer techniques. These experimental methods can provide essential information on the course of macro- and micromixing processes and their characteristic time scales, which can help select the optimal system geometry or operating conditions and validate mixing models. A recent example of this type of research is a work of Kováts et al. (2020), who studied mixing in different coil flow inverters using a fluorescent dye and concluded that an early flow redirection speeds up mixing. On the other hand, Schuler et al. (2021) used X-ray based micro-computed tomography to identify the effect of torsion and curvature of a helical capillary on the evolution of radial concentration profiles of iodine tracer. Studies using mixing sensitive chemical probes are not as popular as the passive tracer methods, but they can provide valuable data on mixing at the molecular scales. For example, Boesinger et al. (2005) determined rapid reduction of the local concentration variances in a curved tube mixer with the chaotic flow for the Reynolds number close to 700 using a fast redox reaction between triiodide and thiosulfate ions. Liang and Zhang (2014) used competitive and consecutive diazo

coupling reactions to prove that mixing in the helical coil can be enhanced by reshaping Dean vortices due to cyclic contraction and expansion of the tube cross-section for the Reynolds number exceeding 500. Rożeń and Kopytowski (2020) applied competitive-parallel reactions, i.e. acid-base neutralisation and alkaline ester hydrolysis, to identify the effect of a periodic flow reorientation and an initial inclination of the contact surface of mixed reactant solutions to the curvature plane of the first pipe bend. The authors also determined that micromixing in periodically redirected chaotic flow accelerates rapidly with the increasing Reynolds number so that the selectivity of the test reactions falls almost to 0 for Re > 1000.

Computational fluid dynamics (CFD) is another valuable tool used in the research on mixing curved tube mixers either as a single method or combined with experiments. Numerical simulations of convective and diffusive mixing provide detailed information on various aspects of mixing, which is challenging to acquire experimentally. For example, Yamagishi et al. (2007) calculated Poincare maps and the stretching rate of material lines for serpentine and spiral mixers and several twisted bend mixers. Positive values of Lapunov exponents, reported in this work, clearly show that chaotic advection can be triggered in a stable laminar flow by its periodic redirection even for medium Reynolds numbers (Re > 200). Mridha et al. (2011) simulated numerically flow and distribution of a passive tracer in a standard helical coil and a system of four short helical coils rotated by 90° angle (coiled flow inverter). They found a distinct improvement of mixing in the second device over the standard helical coil for the comparable pumping costs. Mansour et al. (2017), using CFD, demonstrated the effect of the initial orientation of the interface of mixed fluids to the first pair of Dean vortices; the fastest reduction of concentration variances was achieved when the contact surface was initially perpendicular to the symmetry plane separating Dean vortices. Khot et al. (2019) showed that mixing of a passive tracer could be accelerated in coiled tubes by an early flow inversion, i.e. changing the orientation of the pipe curvature. In this way, it was possible to minimise the effect of the initial orientation of the interface between two mixed fluids. Mansour et al. (2020b) studied mixing in spiral pipes, coiled flow inverters (CFI) and coiled flow reversers (CFR), i.e. coils with periodically switched twist direction (left-handed to right-handed and vice versa). The authors demonstrated that the periodic reorientation of the main flow direction speeded up mixing in a wide range of Reynolds numbers (10 < Re < 3000). The reported mixing efficiency obtained in CFI and CFR units considerably exceeded the mixing efficiency of the helical coil. On the contrary to the helical mixer, CFI and significantly CFR quickly eliminate the effect of the initial orientation of the contact surface of mixed fluids versus the symmetry plane separating Dean vortices. It should be noted that the initial configuration of the intermaterial interface at the entrance of the tube mixer may strongly influence mixing even in static mixers with SMX and KMX elements, known as highly efficient in homogenisation and dispersion operations (Heniche et al., 2005). Verma et al. (2020) presented an interesting CFD study of mixing viscoelastic fluid in coiled pipes and coiled flow inverters by calculating fluid particle trajectories. The authors determined the overlap coefficient of Szymkiewicz–Simpson, which measures the overlap between two finite sets of particles. In this way, they demonstrated that periodic coil rotations by 90° angle speeded up mixing for different Weissenberg numbers compared to the standard helical coil.

Calculations of the concentration field of a passive tracer and mapping its concentration variances at different mixer cross-sections allow to determine mixing indices and segregation scales. It helps to find the optimum operating parameters and mixer geometry for passive mixing operations or mixing chemical reactions with linear kinetics. On the other hand, calculations of trajectories of fluid particles allow to determine residence time distributions, Poincare maps, the stretching rate of material lines and Lapunov exponents, which are pretty helpful in revealing the existence of unmixed regions or the presence of chaotic advection in the system. Unfortunately, it is challenging to predict the yield of fast non-linear kinetics chemical reactions based on these computation techniques. For example, to solve the local material balance of a reactant

$$\frac{\partial c_i}{\partial t} + \sum_{j=1}^{3} \alpha_j \frac{\partial c_i}{\partial x_j} = D_i \frac{\partial^2 c_i}{\partial x_j^2} + r_i \tag{1}$$

one must know the history of the local deformation rates of fluid elements α_j in the reaction zone. Ottino et al. (1979) pointed out that the local deformation rates directly affect the local rate of extension of an infinitesimal material surface. Besides, the generation rate of the new material surface has its upper limit related to the local shear rate. Dividing the actual deformation rate by its maximum value gives the energetic efficiency of mixing (Ottino et al., 1979). Knowing this scalar quantity, one can precisely evaluate any mixer geometry and operating parameters when looking for the best way to obtain the highest yield of the main fast chemical reaction proceeding between initially unmixed substrates at the lowest energy cost.

The main objective of this work was to perform CFD modelling of flow, particle trajectories and then calculate the rate of material surface stretching and the energetic efficiency of mixing in a tubular mixer of curvilinear geometry working in the laminar flow regime. The investigated mixer was constructed from 24 pipe bends of 90° angle twisted alternatively by ±90° angle as shown in Fig. 2. Flow and mixing were modelled for a wide range of the Reynolds number and several initial orientations of a planar material surface versus the curvature axis of the first pipe bend.

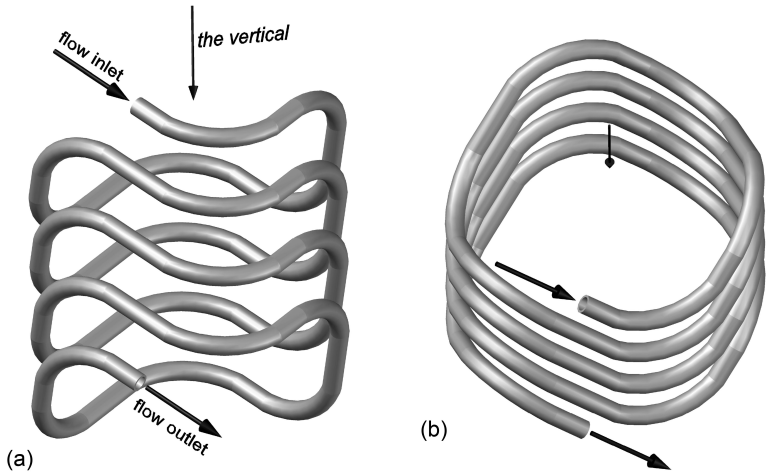

Fig. 2. Twisted bend mixer: (a) sideview, (b) top view

2. QUANTIFICATION OF MIXING

Fluid mixing is a complex process that different mathematical methods can characterise. A suitable choice of the description method usually depends on the expected result of mixing, e.g., narrowing the scatter of the residence time of fluid elements, decreasing the size of unmixed lumps of fluid, reducing the concentration variance of a mixture component and increasing the yield of a chemical reaction. A selection of the description method should also be correlated with either known or assumed a priori mechanism of mixing. Mixing on the molecular scale (micromixing) in the laminar flow is controlled by two processes: extension of the contact surface of mixed fluids and molecular diffusion of mixture components (Bałdyga et al., 1998). The generation rate of a new contact surface area depends on the deformation rate of fluid elements containing this surface and the surface orientation to the principal axes of deformation. Material lines and surfaces extend at the fastest pace in the vicinity of stagnation points, where the trajectories of fluid particles move away at an exponential rate.

In general, the rate of change of an infinitesimal vector connecting two fluid particles reads

$$\frac{\mathrm{d}}{\mathrm{d}t}\left(\mathrm{d}\vec{l}\right) = \mathrm{d}\vec{l}\cdot\nabla\vec{v} \tag{2}$$

The rate of volume change of a fluid element equals

$$\frac{\mathrm{d}}{\mathrm{d}t}(\mathrm{d}V) = (\nabla\cdot\vec{v})\,\mathrm{d}V \tag{3}$$

The volume of the fluid element can be expressed as the scalar product of vectors representing the material line and surface

$$\mathrm{d}V = \mathrm{d}\vec{A} \cdot \mathrm{d}\vec{l} \tag{4}$$

Differentiating Eq. (4) and combining it with Eqs. (2) and (3) leads to the expression for the rate of change of the material surface vector

$$\frac{\mathrm{d}}{\mathrm{d}t}\left(\mathrm{d}\vec{A}\right) = (\nabla \cdot \vec{v})\,\mathrm{d}\vec{A} - \nabla\vec{v} \cdot \mathrm{d}\vec{A} \tag{5}$$

Ottino et al. (1979) demonstrated that the stretching rate of the infinitesimal surface area reads

$$\alpha = \frac{1}{\left|\mathrm{d}\vec{A}\right|} \cdot \frac{\mathrm{d}\left|\mathrm{d}\vec{A}\right|}{\mathrm{d}t} = \theta - \overline{\overline{D}} : \vec{n}\vec{n} \tag{6}$$

where θ is the rate of the volumetric strain, $\vec{n}$ is the unit direction vector, and $\overline{\overline{D}}$ is the rate of deformation tensor:

$$\theta = \nabla \cdot \vec{v} \tag{7}$$

$$\vec{n} = \frac{\mathrm{d}\vec{A}}{\left|\mathrm{d}\vec{A}\right|} \tag{8}$$

$$\overline{\overline{D}} = \frac{1}{2}\left(\nabla\vec{v} + \nabla\vec{v}^{T}\right) \tag{9}$$

Introducing Eqs. (6) and (8) into Eq. (5) gives

$$\frac{\mathrm{d}\vec{n}}{\mathrm{d}t} = \left(\overline{\overline{D}} : \vec{n}\vec{n}\right)\vec{n} - \nabla\vec{v} \cdot \vec{n} \tag{10}$$

Equation (10) has to be integrated along the trajectory of the centre of the surface $\mathrm{d}\vec{A}$ to compute the stretching rate of the surface area, α, from Eq. (6). The stretching rate of the surface area is by its nature an invariant of rotation and can be expressed by the principal rates of strain (Aris, 1989)

$$\alpha = \theta - \sum_{j=1}^{3} \alpha_j n_j^2 = \frac{2}{3}\theta - \sum_{j=1}^{3}\left(\alpha_j - \frac{1}{3}\theta\right) n_j^2 \tag{11}$$

Taking into account the following obvious equalities:

$$\sum_{j=1}^{3} n_j^2 = 1 \tag{12}$$

$$\sum_{j=1}^{3}\left(\alpha_j - \frac{1}{3}\theta\right) = 0 \tag{13}$$

one can apply Ostrowski's inequality (Mitrinović et al., 1993) to find out that

$$\left[\sum_{j=1}^{3}\left(\alpha_j - \frac{1}{3}\theta\right) n_j^2\right]^2 \leq \left(\sum_{j=1}^{3} n_j^4 - \frac{1}{3}\right) \cdot \sum_{j=1}^{3}\left(\alpha_j - \frac{1}{3}\theta\right)^2 \leq \frac{2}{3}\sum_{j=1}^{3}\left(\alpha_j - \frac{1}{3}\theta\right)^2 \tag{14}$$

On the other hand, the dissipation rate of mechanical energy by viscous forces reads

$$\varepsilon = 2\mu \sum_{j=1}^{3}\left(\alpha_j - \frac{1}{3}\theta\right)^2 = 2\mu\dot{\gamma}^2 \tag{15}$$

Hence, the stretching rate of the surface area has an upper bound, which is determined by the rate of volumetric strain (in incompressible flow $\theta = 0$) and the shear rate.

$$\alpha_{\max} = \frac{2}{3}|\theta| + \frac{1}{\sqrt{3}}\dot{\gamma} \tag{16}$$

Next, following Ottino et al. (1979), one can define the energetic efficiency of mixing

$$\mathrm{eff} = \frac{\alpha}{\alpha_{\max}} \tag{17}$$

Rożeń (2008) pointed out that the denominator in Eq. (17) is too large because the authors applied general Cauchy-Schwarz inequality instead of specific Ostrowski's inequality to calculate $\alpha_{\max}$. As a result, the energetic efficiency of any natural flow could not exceed $\sqrt{2/3}$. If the upper bound of the surface area stretching is calculated according to Eq. (16), $|\mathrm{eff}| \leq 1$; $\mathrm{eff} = \pm 1$ is achieved in the axially symmetric stagnation flow.

Let the motion of fluid particles in a system be denoted by

$$\vec{x} = \vec{X}^{+}(\vec{x}_0, t) \tag{18}$$

and let us follow the fluid particle P, which was in point $\vec{x}_0$ at $t = 0$. If an infinitesimal material surface $\mathrm{d}\vec{A}$ around P is deformed at rate $\alpha\left[\vec{X}^{+}(\vec{x}_0, t)\right]$, then its area at time t reads

$$\mathrm{d}A = \mathrm{d}A_0\, e^{\langle \alpha_P \rangle t} \tag{19}$$

where

$$\langle \alpha_P \rangle = \frac{1}{t} \cdot \int_0^t \alpha\left[\vec{X}^{+}(\vec{x}_0, t')\right] \mathrm{d}t' \tag{20}$$

Consequently, the area of a finite material surface changes upon deformation from A_0 at $t = 0$ to a new value

$$A(t) = \iint_{A_0} e^{\langle \alpha_P \rangle t}\, \mathrm{d}A_0 \tag{21}$$

The deformation rate of the material surface and its time average read:

$$\alpha_A(t) = \frac{\mathrm{d}}{\mathrm{d}t}\ln[A(t)] = \frac{\iint_{A_0} \alpha\left[\vec{X}^{+}(\vec{x}_0, t)\right] \cdot e^{\langle \alpha_P \rangle t}\, \mathrm{d}A_0}{\iint_{A_0} e^{\langle \alpha_P \rangle t}\, \mathrm{d}A_0} \tag{22}$$

$$\langle \alpha_A \rangle = \frac{1}{t} \cdot \int_0^t \alpha_A(t')\, \mathrm{d}t' \tag{23}$$

The energetic efficiency of stretching of the finite material surface and its time average can be estimated using similar Lagrangian approach:

$$\mathrm{eff}_A(t) = \frac{1}{A}\iint_A \mathrm{eff}(\vec{x})\, \mathrm{d}A = \frac{\iint_{A_0} \mathrm{eff}\left[\vec{X}^{+}(\vec{x}_0, t)\right] \cdot e^{\langle \alpha_P \rangle t}\, \mathrm{d}A_0}{\iint_{A_0} e^{\langle \alpha_P \rangle t}\, \mathrm{d}A_0} \tag{24}$$

$$\langle \alpha_A \rangle = \frac{1}{t} \int_0^t \mathrm{eff}_A(t')\,\mathrm{d}t' \tag{25}$$

When two fluids are mixed in a tubular mixer, their contact surface is constantly created at the mixer inlet and then stretched during mixing. The contact surface area per volume of the fluid element comprising this surface changes as follows

$$a_V\left[\vec{X}^+(\vec{x}_0,t)\right] = a_V\left[\vec{X}^+(\vec{x}_0,0)\right] \cdot e^{\langle \alpha_P \rangle t} \tag{26}$$

Hence, the total area stretch reached in the mixer with the steady flow reads

$$\eta = \frac{\iint\limits_{S_2} a_V(\vec{x}) \cdot \vec{v}(\vec{x}) \cdot \mathrm{d}\vec{S}}{\iint\limits_{S_1} a_V(\vec{x}_0) \cdot \vec{v}(\vec{x}_0) \cdot \mathrm{d}\vec{S}} = \frac{\iint\limits_{S_1} a_V(\vec{x}_0) \cdot e^{\langle \alpha_P \rangle t} \cdot \vec{v}(\vec{x}_0) \cdot \mathrm{d}\vec{S}}{\iint\limits_{S_1} a_V(\vec{x}_0) \cdot \vec{v}(\vec{x}_0) \cdot \mathrm{d}\vec{S}} \tag{27}$$

where S_1 and S_2 are the mixer inlet and outlet surfaces, and t is the residence time of the fluid element in the system. In this case, the mean flow energetic efficiency of mixing can be estimated as follows:

$$\langle\langle \mathrm{eff} \rangle\rangle = \frac{\iint\limits_{S_2} \langle \mathrm{eff}_P \rangle \cdot a_V(\vec{x}) \cdot \vec{v}(\vec{x}) \cdot \mathrm{d}\vec{S}}{\iint\limits_{S_2} a_V(\vec{x}) \cdot \vec{v}(\vec{x}) \cdot \mathrm{d}\vec{S}} = \frac{\iint\limits_{S_1} \langle \mathrm{eff}_P \rangle \cdot a_V(\vec{x}_0) \cdot e^{\langle \alpha_P \rangle t} \cdot \vec{v}(\vec{x}_0) \cdot \mathrm{d}\vec{S}}{\iint\limits_{S_1} a_V(\vec{x}_0) \cdot e^{\langle \alpha_P \rangle t} \cdot \vec{v}(\vec{x}_0) \cdot \mathrm{d}\vec{S}} \tag{28}$$

where

$$\langle \mathrm{eff}_P \rangle = \frac{1}{t} \int_0^t \mathrm{eff}\left[\vec{X}^+(\vec{x}_0,t'),t'\right] \mathrm{d}t' \tag{29}$$

is the time average of the energetic efficiency of mixing in the fluid element.

Quantities defined in this chapter and a classical residence time distribution technique were applied in a sensitivity study of computation grids and later in a parametric study of mixing in the twisted bends reactor.

3. COMPUTATIONAL FLUID DYNAMICS

Flow and mixing simulations were carried out for the twisted bend mixer illustrated in Fig. 2. This tubular mixer is constructed from 24 pipe bends of 90° angle twisted in an alternating manner by ±90° angle to induce chaotic advection. There are 3 mm and 33 mm straight sections inserted alternately between the bends to create a coil-like structure instead of making a closed loop from the pipe sections. The pipe diameter is $d = 0.012$ m, and the curvature radius of the bends is $R_c = 0.075$ m, which gives the curvature ratio $\delta = 0.08$. The total length of the mixer equals 3.295 m. The geometry of the studied mixer imitates the geometry of the twisted bend reactor used in experiments with competitive-parallel chemical reactions by Rożeń and Kopytowski (2018; 2020). The actual length of the tube mixer was selected to reduce the average size of unmixed fluid volumes to approximately 10^{-8} m, even for the lowest flow rates.

Computations were conducted for a steady-state, isothermal, and incompressible flow of liquid having the physical properties of water at 22 °C ($\rho = 997.77$ kg/m^3, $\mu = 9.544 \cdot 10^{-4}$ Pa · s). The flow conditions in

the mixer were characterised by the Reynolds and Dean numbers:

$$\mathrm{Re} = \frac{\bar{v} d \rho}{\mu} \tag{30}$$

$$\mathrm{De} = \mathrm{Re}\sqrt{\delta} \tag{31}$$

Some flow data used in the flow and mixing simulations are presented in Table 1.

Table 1. Reynolds number, Dean number, mean velocity, mean residence time

Re	20	50	100	200	500	1000	2000
De	5.66	14.14	28.28	56.57	141.42	282.84	565.68
$\bar{v}$ [m/s]	0.00159	0.00399	0.00797	0.01594	0.03986	0.07971	0.15942
$\bar{t}$ [s]	2067.11	826.84	413.42	206.71	82.68	41.34	20.67

The CFD Ansys Fluent 2020 R1 software was used in the present study in flow simulations. The continuity and momentum equations:

$$\frac{\partial v_i}{\partial x_i} = 0 \tag{32}$$

$$\sum_{j=1}^{3} v_j \frac{\partial v_i}{\partial x_j} = -\frac{1}{\rho}\frac{\partial p}{\partial x_i} + \frac{\mu}{\rho}\sum_{j=1}^{3}\frac{\partial^2 v_i}{\partial x_j^2} \tag{33}$$

were solved utilising the pressure-based and steady-state solver. Non-slip boundary condition was applied at the tube walls, and the parabolic velocity profile with the mean velocity $\bar{v}$ was set at the mixer inlet. The SIMPLE algorithm was used for pressure-velocity coupling and the Least Squares Cell-Based Gradient evaluation scheme, the second-order interpolation scheme for pressure, and the second-order upwind scheme for velocity. The numerical solution was considered converged when the continuity equation's residual fell below 10^{-6}, and the residuals of momentum equations fell below 10^{-8}.

According to Mansour et al. (2020a), who formulated general guidelines for meshing techniques for tubular mixers of curved geometry, the optimal choice is a structured grid with hexahedral cells aligned with the main flow direction. Hence, three such grids of different densities were used in computations. The three-dimensional grids were created by sweeping two-dimensional grids along the curvilinear channel. All grids were refined near the channel walls to resolve high gradients of fluid velocity present in this region. The coarse grid has 1.776 million cells, the medium grid has 5.994 million cells, and the most refined grid has 14.256 million cells. The cross-sections of the computational grids are shown in Fig. 3. The number of cells in the pipe cross-section, m_{xy}, and along one "coil" turn made from six pipe bends, m_z, are reported in Table 2, along with the mean cell size in the transverse, $\bar{\Delta}_{xy}$, and the axial direction, $\bar{\Delta}_z$.

Table 2. Details of the computational grids

Grid no	m_{xy}	m_z	$\bar{\Delta}_{xy}$ [mm]	$\bar{\Delta}_z$ [mm]
1	500	888	0.475	0.942
2	1125	1332	0.317	0.628
3	2000	1782	0.238	0.469

Grid sensitivity tests were carried out for various aspects of flow and mixing in the twisted bend mixer to determine the possible application range of each grid.

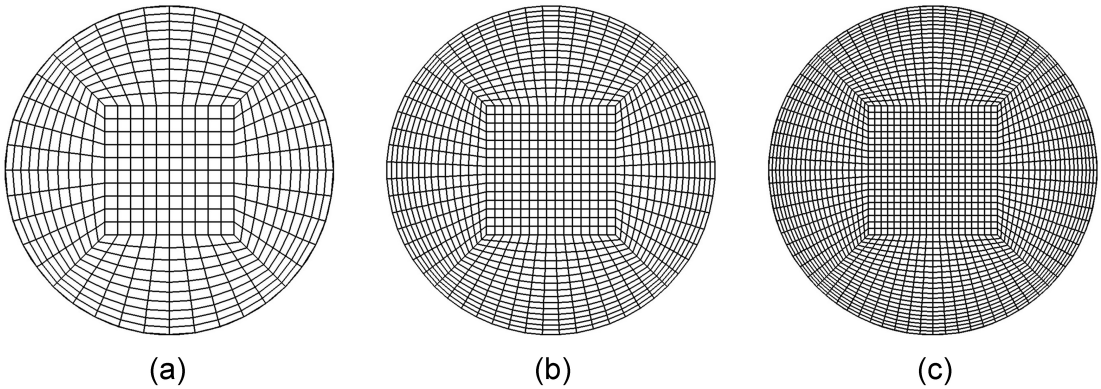

Fig. 3. Cross-sections of computational grids: (a) grid 1, (b) grid 2, (c) grid 3

First, the effect of the grid resolution on the head loss and the velocity field was determined. Table 3 shows that the Fanning friction factor values calculated for the same Reynolds numbers are close for all tested grids. The difference between results obtained for the grids 1 and 3 increases from 0.2% for Re = 20 to 1.2% for Re = 2000. Furthermore, there are small differences between the friction coefficients determined in CFD simulations and those calculated from the Manlapaz and Churchill correlation for the toroidal channel of the same curvature as the twisted pipe bends. Figure 4 presents the friction factor versus Reynolds number obtained for grid no 3 and the friction factor of the equivalent helical coil and the straight pipe. The helical coil had the same pitch as the twisted bend mixer (57.2 mm), and the coil radius was set to 121.1 mm, i.e., the average distance of the pipe centreline from the main axis of the twisted bends mixer. As can be seen, the friction factor of the twisted bend mixer is slightly higher than that of the equivalent helical coil. This difference increases with the increasing Reynolds number up to 10% for Re = 2000 and

Table 3. Friction factor computed for the pipe mixer (this work) and the toroidal pipe of the same curvature as the pipe bends from the correlation by Manlapaz and Churchill (1981)

Re	20	50	100	200	500	1000	2000
Grid 1	0.8012	0.3260	0.1779	0.1027	0.05330	0.03389	0.02216
Grid 2	0.8023	0.3264	0.1781	0.1027	0.05323	0.03378	0.02203
Grid 3	0.8026	0.3264	0.1783	0.1029	0.05329	0.03374	0.02190
Correlation	0.8043	0.3261	0.1770	0.1035	0.05246	0.03347	0.02244

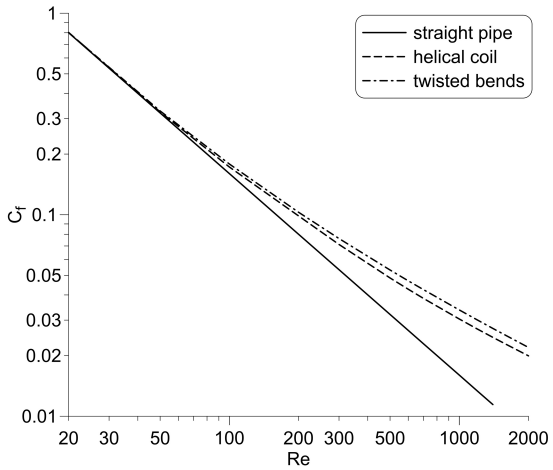

Fig. 4. Fanning friction factor of different tube mixers

is six times smaller than the difference between the friction factors of the straight pipe and the twisted bend mixer. Hence, it can be concluded that frequent redirection of the main flow, aimed to induce chaotic advection, has a minimal effect on the actual pumping costs.

Figures 5 and 6 show a comparison of the normalised velocity profiles calculated for the tested grids. There is little difference between these profiles at the low Reynolds number, but as the Reynolds number equals 1400, differences become visible almost in the entire profile span. However, the mean differences between the axial velocity profiles ($v_z/\bar{v}$) calculated for grids 2 and grid 3 are lower than 1.5% of $\bar{v}$ even for Re < 1600, as reported in Table 4, despite significant changes in the shape of the velocity profiles with the increasing Reynolds number. The velocity profiles calculated for the twisted bend mixer are similar to those obtained for a typical helical coil (Kumar et al., 2006), only for the low Reynolds numbers (Re ≤ 500).

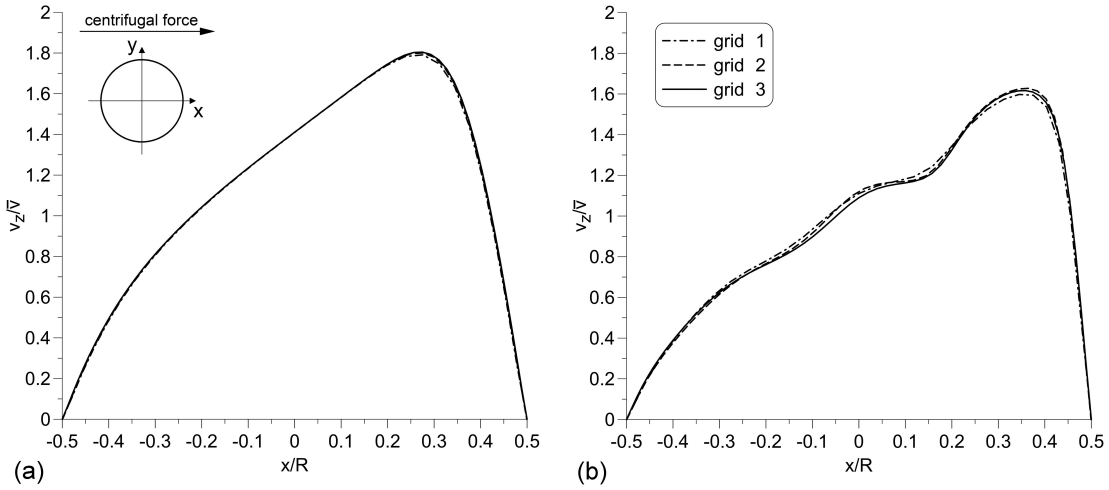

Fig. 5. Profiles of the axial velocity component in the channel cross-section between 19th and 20th pipe bend: (a) Re = 200, (b) Re = 1400

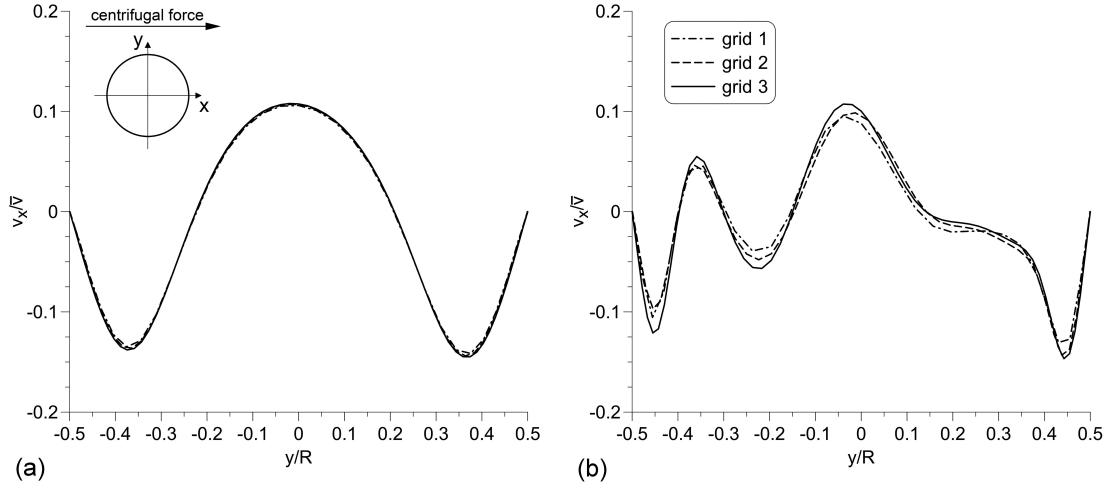

Fig. 6. Profiles of the transversal velocity component in the channel cross-section between 19th and 20th pipe bend: (a) Re = 200, (b) Re = 1400

The effect of the grid resolution of the residence time distribution of fluid elements was evaluated in the next step. The residence time distribution (RTD), or in other words, the exit age time distribution, allows to study the longitudinal dispersion of fluid particles in the system. In the present work, RTDs were obtained by solving the trajectory equation

$$\frac{\mathrm{d}\vec{x}}{\mathrm{d}t} = \vec{v}\,(\vec{x})\,, \qquad \vec{x} = \vec{x}_0 \quad \text{at} \quad t = 0 \tag{34}$$

Table 4. Mean difference between the normalised axial velocity profiles ($v_z/\bar{v}$) obtained for grids 1 and 2 and the normalised velocity profile determined for grid 3

Re	20	50	100	200	500	1000	1200	1400	1600
Grid 1	0.0107	0.0109	0.0122	0.0132	0.0146	0.0129	0.0196	0.0224	0.0223
Grid 2	0.0058	0.0059	0.0065	0.0069	0.0077	0.0077	0.0102	0.0144	0.0107

for 16384 massless particles injected at evenly distributed locations at the mixer inlet. Equation (34) was integrated within the Fluent post-processing module employing a Runge-Kutta method. The distance covered by the fluid particle during each time integration step was limited by the size of the passed grid cell. Figure 7 compares the RTD histograms, plotted versus dimensionless residence time, $\tau = t/\bar{t}$, for all tested grids and two Reynolds numbers. As expected, the residence time distributions become more concentrated around the mean residence time with the increasing Reynolds number. It can also be seen that the histograms obtained for low and medium-resolution grids 1 and 2 are close to that determined for the highest resolution grid 3 for Re = 200. When the Reynolds number equals 1400, the maxima of the histograms obtained for grids 1 and 2 are higher than that determined for grid 3.

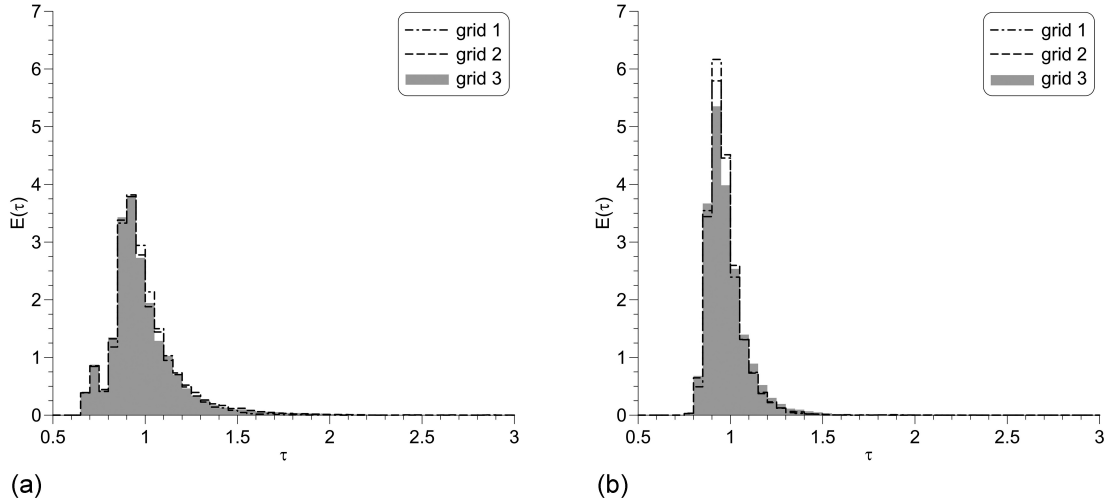

Fig. 7. Dimensionless residence time distribution function: (a) Re = 200, (b) Re = 1400

To quantify the mesh discretisation error, the mean differences between the RTD obtained for grids 1, and 2 and the RTD determined for grid 3 were calculated and listed in Table 5. As can be seen, the difference in the RTDs obtained for grids 1, and 3 stays in 8–12% interval if Re ≥ 500. However, the difference in the RTDs for grids 2 and 3 is approximately two times smaller and exceeds 4% not until Re ≥ 1000.

Table 5. Mean differences between the residence time distributions obtained for grids 1 and 2 and the residence time distribution determined for grid 3

Re	20	50	100	200	500	1000	1200	1400	1600
Grid 1	0.0144	0.0587	0.0274	0.0370	0.0773	0.1168	0.0850	0.0859	0.1199
Grid 2	0.0074	0.0212	0.0167	0.0183	0.0173	0.0414	0.0398	0.0654	0.0466

Finally, the effect of the grid resolution on the energetic efficiency of mixing was determined. All the calculations were carried out for a planar material surface, which was initially aligned with the parabolic flow and inclined by a 90° angle to the curvature plane of the first pipe bend. The linear intersection of the material surface and the mixer inlet in Fig. 8 was divided into 1024 equal segments. The trajectory of

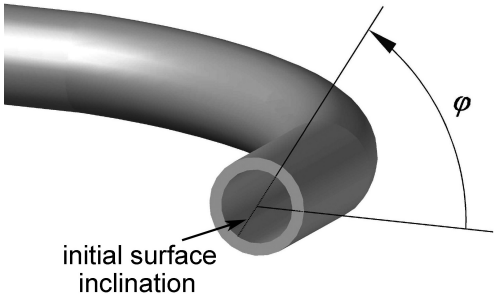

Fig. 8. The intersection of the material surface with the mixer inlet

the fluid particle located centrally in the k-th segment at point $\vec{x}_{0,k}$ was calculated by integrating Eq. (34). All components of the velocity gradient tensor $\nabla\vec{v}$ were extracted at each computed position of the fluid particle from the numerical solution of the flow field and exported to a data file within the Fluent post-processing module. These data were then used to integrate Eq. (10) along the particle trajectory, calculate the stretching area rate from Eq. (6) and the energetic efficiency of mixing from Eq. (17). The Runge-Kutta method was applied to numerically integrate Eq. (10) with the initial condition stating that the unit vector $\vec{n}$ is perpendicular to the material surface at the mixer inlet. The stretching rate of the material surface, $\alpha_A(t)$, and the energetic efficiency of this process, $\mathrm{eff}_A(t)$, were calculated by approximating integrals in Eqs. (22) and (24) with finite sums over all segments of the material surface:

$$\alpha_A(t) \cong \frac{\sum_k \alpha\left[\vec{X}^+\left(\vec{x}_{0,k},t\right)\right]\cdot e^{\langle\alpha_{P,k}\rangle t}}{\sum_k e^{\langle\alpha_{P,k}\rangle t}} \tag{35}$$

$$\mathrm{eff}_A(t) \cong \frac{\sum_k \mathrm{eff}\left[\vec{X}^+\left(\vec{x}_{0,k},t\right)\right]\cdot e^{\langle\alpha_{P,k}\rangle t}}{\sum_k e^{\langle\alpha_{P,k}\rangle t}} \tag{36}$$

where $\langle\alpha_{P,k}\rangle$ is the time average stretching rate of the k-th fragment of the intersection of the material surface at the mixer inlet.

A comparison of time-averaged energetic efficiency of mixing obtained for all tested grids, presented in Fig. 9, indicates that the grid resolution significantly impacts the energetic efficiency of mixing. The results obtained for the coarse grid 1 diverge from results obtained for grids 2 and 3 for Re ≥ 200, and when

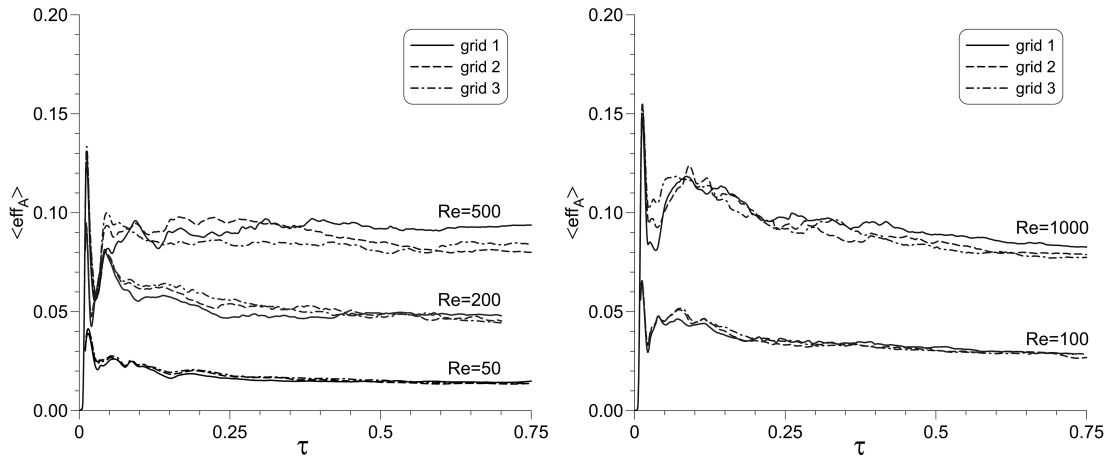

Fig. 9. Effect of the grid resolution on the time-averaged energetic efficiency of mixing

Re ≥ 500, it is true even for the long times ($\tau > 0.5$). Differences between results obtained for the medium grid 2 and the most refined grid 3 increase for Re ≥ 500. The long-time values of the energetic efficiency of mixing obtained for grids 2 and 3 remain close to each other for Re ≤ 1000.

The grid sensitivity study shows that differences between RTDs and the energetic efficiencies of mixing calculated for the examined grids rise quickly with the increasing Reynolds number due to the presence of chaotic advection in the twisted bend mixer. In such a case, even minor errors of the numerical solution of the velocity field may result in exponentially growing errors of the numerical integration of fluid particle trajectories (Souvaliotis et al., 1995). Increasing the grid density can reduce the computational domain discretisation error and the time integration error. On the other hand, using too dense grids may lead to prohibitively long computation times and the growth of round-off errors. Nevertheless, a correct determination of trends followed by the statistical properties of a dynamical system is still possible due to the so-called shadowing phenomenon. According to Palmer (2009), an approximate fluid particle trajectory determined by numerical integration is shadowed by an accurate fluid particle trajectory in the flow system with chaotic advection. Therefore, applying the statistical tools to mixing quantities, e.g. calculation of the population, time or flow average, should help identify the optimal processing conditions in the tube mixers of curvilinear geometry and chaotic advection. All numerical simulations of mixing, whose results are presented in the next chapter, were carried out using the highest resolution grid 3 for Re ≤ 1200.

4. RESULTS AND DISCUSSION

The deformation rate of fluid elements and the stretching rate of an inter material surface in these elements depends on the total system throughput in a continuous flow tube mixer. This obvious relation is sometimes complex and subject to different conditions such as hydrodynamic instability, chaotic advection, or transition to different flow regimes. Apart from that, higher total throughput leads to higher shear rates and pumping costs. Hence, it is essential to know whether changing the flow rate is indeed energetically efficient in reducing segregation scales or concentration variances of mixture components. Finding the optimum flow conditions for mixing becomes even more complicated when mixing is accompanied by fast chemical reactions of non-linear kinetics and proceeds between initially unmixed reactants. Knowledge on how the contact surface area changes with time and how effective mechanical energy is spent during this process can be beneficial in the search for the highest final product output and purity at the lowest energetic cost.

In this work, time-averaged values of the stretching rate of the material surface and the energetic efficiency of mixing were calculated for the twisted bend mixer. The mixing simulations were carried for different Reynolds numbers and various initial orientations of the material surface at the mixer inlet.

First, the material surface entering the mixer is assumed to be aligned with the parabolic flow at the mixer inlet. It is also perpendicular to the curvature plane of the first pipe bend ($\varphi = 90°$). Results presented in Fig. 10 indicate that in this case, the fastest stretching of the material surface occurs immediately after this surface enters the first pipe bend. The maximum stretching rate is observed because the material surface, initially perpendicular to the symmetry plane between the first two counter-rotating Dean vortices, is quickly entrained, rotated and deformed by the vortices. After some time, the material surface becomes aligned with the shearing flow and the deformation rate decreases. However, when the material surface flows into the next pipe bend twisted by 90° angle, it experiences a rapid reorientation and a new stretching burst. This process repeats itself, creating the subsequent local maxima and minima of the stretching rate, but the material surface's longitudinal dispersion eventually dumps these oscillations. Comparing the long-time stretching rates normalised by the mean pipe velocity shows that the new material surface's generation rate is not proportional to the Reynolds number. The long-time stretching rate increases faster

than the Reynolds number almost in the entire tested range, and the most significant gains are observed when Re ≤ 100.

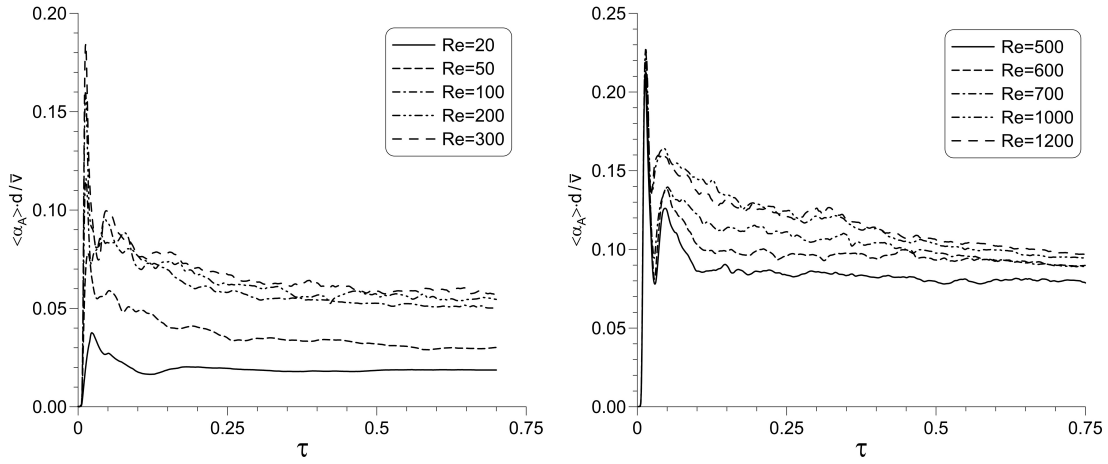

Fig. 10. Effect of the Reynolds number on the time-averaged rate of stretching of the material surface for $\varphi = 90°$

The time average energetic efficiency of mixing is presented in Fig. 11. In this case, the highest efficiency is also observed immediately after the material surface enters the first pipe bend. It should be noted that when Re ≥ 500, the global maximum of the energetic efficiency exceeds 0.15. The long-time energetic efficiency of mixing cannot be so high. Anyway, the highest long-time energetic efficiency close to 0.1 is observed for Re = 700. It is a good result for any mixer which can be used in industrial practice. Further increase of the Reynolds number rapidly reduces the long-time energetic efficiency of mixing.

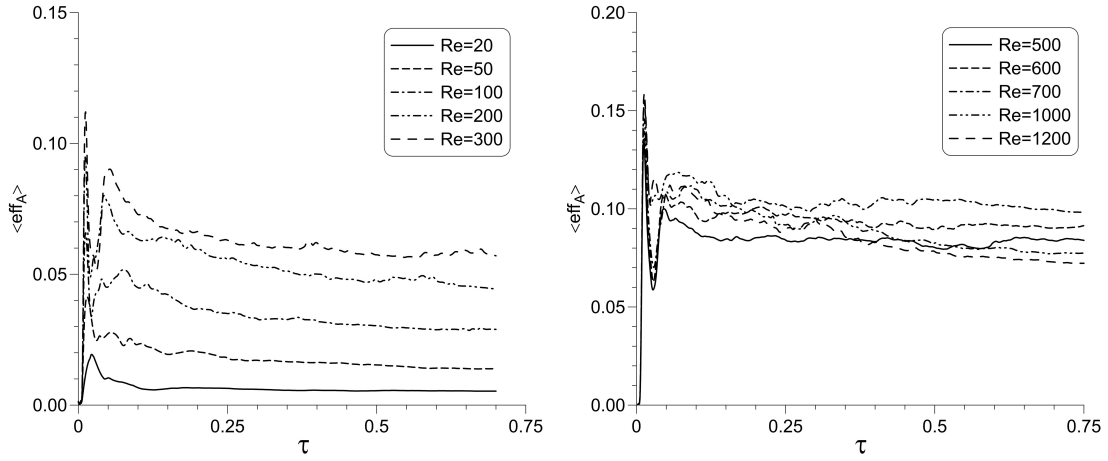

Fig. 11. Effect of the Reynolds number on the time-averaged energetic efficiency of mixing of the material surface for $\varphi = 90°$

Let us now see how fast and energetically effective is the generation of the new material surface when the surface is not initially perpendicular to the curvature plane of the first pipe bend ($\varphi \neq 90°$). The results presented in Fig. 12 for two Reynolds numbers 300 and 700 show that the worst initial orientation of the material surface is when this surface coincides with the symmetry plane separating the first pair of Dean vortices ($\varphi = 0°$). Shortly after the material surface enters the first pipe bend, a rapid reduction of the surface area is observed instead of an extension when $\varphi = 0°$. Eventually, the stretching rate becomes positive for $\tau \approx 0.04$, i.e. when the material surface leaves the first pipe bend; the mean dimensionless residence time in each of 24 pipe bends equals 0.042. The time average stretching rate becomes practically independent of the initial orientation of the material surface to the Dean flow for Re = 300 if $\tau > 0.3$ and for Re = 700 if $\tau > 0.5$. Unfortunately, this is not true in the case of the time average energetic efficiency

of mixing. Results presented in Fig. 13 allow to conclude that the highest energetic efficiency of mixing is achieved for $\varphi = 90°$ and the lowest one for $\varphi = 0°$. The negative values of the energetic efficiency obtained for $\varphi = 0°$ in the first pipe bend follow from the negative values of the stretching rate reported in Fig. 12. In the case of the two remaining angles, 45° and 135°, the time-averaged energetic efficiency of mixing is always positive. Still, its long-time value is smaller than that obtained for the optimum inclination angle. A similar influence of the initial orientation of the contact surface on the rate of mixing of passive traces in the tubular mixers of curved geometry (helical coils, inverted pipe bends, CFI and CFR) was earlier reported by Mansour et al. (2017; 2020b) and Khot et al. (2019). Rożeń and Kopytowski (2020) recently confirmed this effect for reactive mixing in the twisted bend mixer.

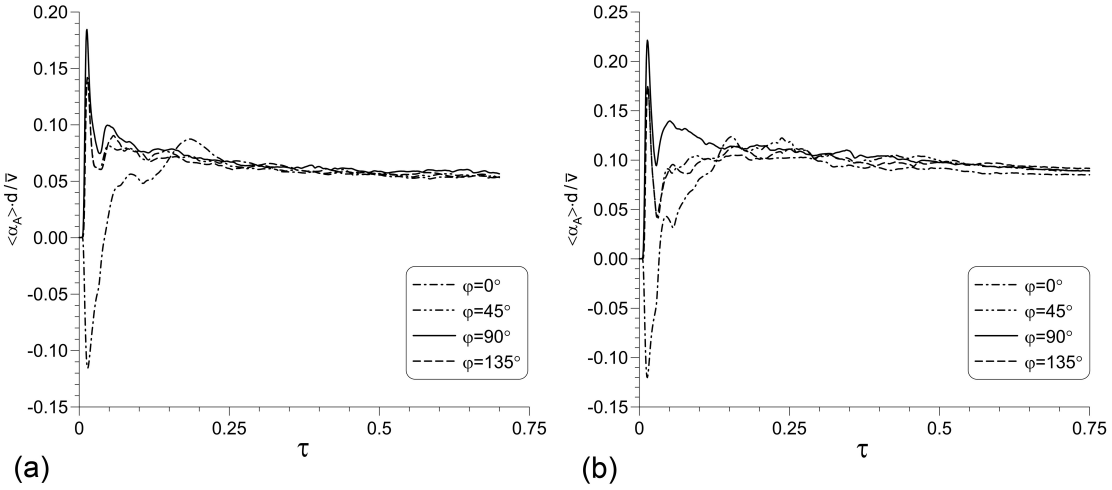

Fig. 12. Effect of the initial inclination of the material surface to the curvature plane of the first pipe bend on the time-averaged stretching rate: (a) Re = 300, (b) Re = 700

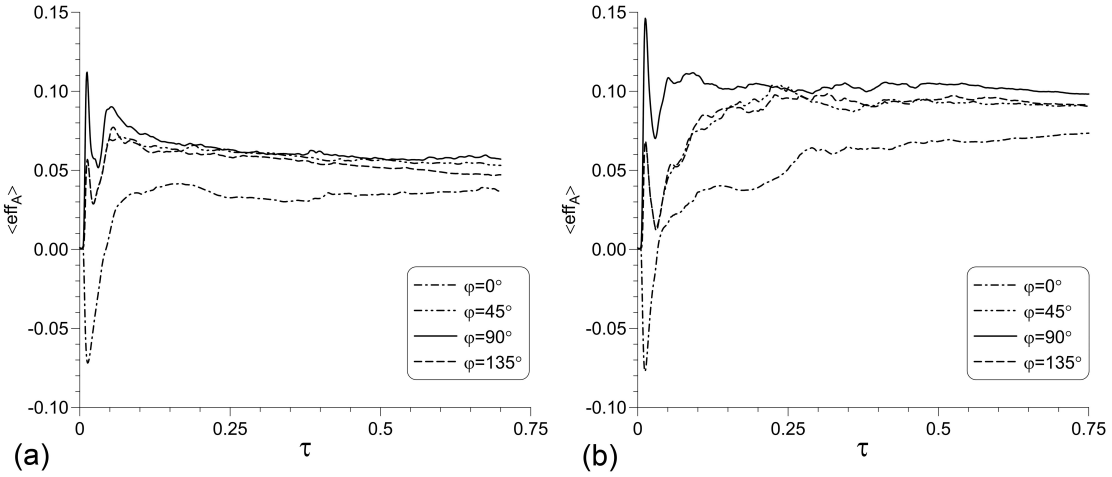

Fig. 13. Effect of the initial inclination of the material surface to the curvature plane of the first pipe bend on the time-averaged energetic efficiency of mixing: (a) Re = 300, (b) Re = 700

Finally, the total area stretch of the material surface and the flow average energetic efficiency of mixing were calculated. The integrals in Eqs. (27) and (28) were approximated in the calculations by the finite sums:

$$\eta \cong \frac{\sum_k e^{\langle \alpha_{P,k} \rangle t_k} \cdot v\left(\vec{x}_{0,k}\right)}{\sum_k v\left(\vec{x}_{0,k}\right)} \tag{37}$$

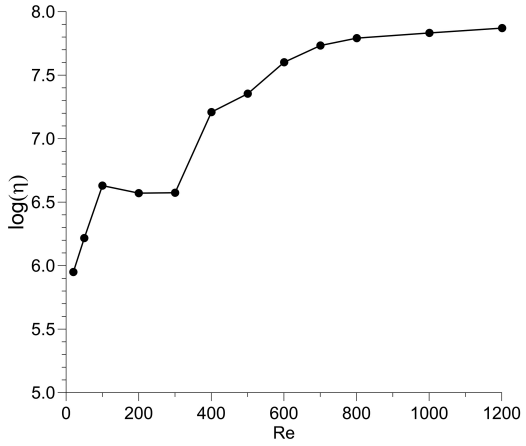

Fig. 14. Total surface area stretch at the mixer exit ($\varphi = 90°$)

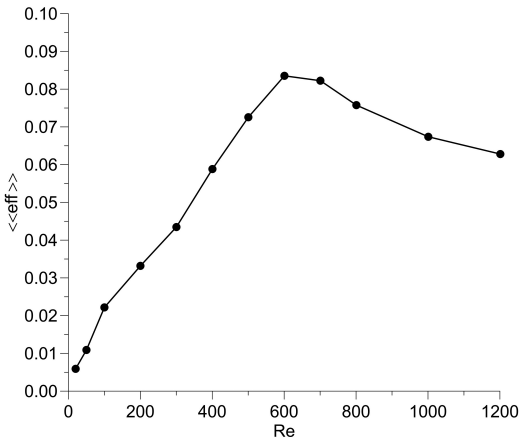

Fig. 15. Mean energetic efficiency of mixing at the mixer exit ($\varphi = 90°$)

$$\langle\langle \text{eff} \rangle\rangle \cong \frac{\sum_k \langle \text{eff}_{P,k} \rangle \cdot e^{\langle \alpha_{P,k} \rangle t_k} \cdot v\left(\vec{x}_{0,k}\right)}{\sum_k v\left(\vec{x}_{0,k}\right)} \tag{38}$$

where t_k is the residence time of the k-th segment of the intersection of the material surface and the mixer inlet, $v\left(\vec{x}_{0,k}\right)$ is the velocity of the k-th segment at the mixer inlet, and all segments have the same size.

The common logarithm of the total area extension of the material surface obtained for the twisted bend mixer is plotted in Fig. 14 versus the Reynolds number. These results indicate that the entire area stretch increases with the increasing Reynolds number except for the region where $100 < \text{Re} < 300$. Kováts et al. (2020) also reported slower mixing of a passive tracer in this range of the Reynolds numbers for CFR mixers. Furthermore, according to the continuity condition, the growth of the material area should be inversely proportional to the mean size of the unmixed fluid volumes (e.g. drops, striations) at any pipe cross-section, including the mixer outlet. It allows to conclude that convective mixing can reduce the segregation scale by six to eight orders of magnitude. Hence, if the initial segregation scale is close to the pipe radius and the Reynolds number approaches 1000, it will homogenise fluid components at the molecular level.

The flow average energetic efficiency of mixing calculated for the material surface extended in the twisted bend mixer is presented in Fig. 15. As can be seen, the energetic efficiency of mixing has a global maximum at $\text{Re} \approx 600$. Any further increase in Reynolds number will accelerate mixing and create more material surface area but at a proportionally higher energetic cost.

5. CONCLUSIONS

Numerical simulations of laminar flow and convective mixing have been carried out for a tube mixer of curved geometry. The mixer was constructed from pipe bends of 90° angle twisted in an alternating manner by ±90° angle. In such a system, the main flow direction is periodically reoriented, and Dean vortices creating the secondary flow in the curved tubes are regularly destroyed and formed again. As a result, chaotic advection is developed in steady three-dimensional laminar flow, and the new inter material surface area is created faster.

The head loss calculated for the twisted bend mixer does not differ significantly from the head loss characterising flow in a toroidal channel of the same curvature ratio. Sensitivity tests performed for three

grids with hexahedral cells and different densities showed that minor differences in the approximation of the velocity field might translate into significant differences in calculations of the residence time distribution and the energetic efficiency of mixing in the tube mixer with chaotic advection.

Practical procedures of calculating the extension rate of a finite material surface, the energetic efficiency of this mixing process, the total surface area stretch achieved in the mixer and the flow average of the energetic efficiency of mixing were proposed and applied. Mixing calculations were done for a wide range of the Reynolds numbers and several initial orientations of the material surface to Dean flow in the first pipe. It was found that the stretching rate of the material surface did not increase proportionally to the increasing Reynolds number, and it was susceptible to the initial inclination of the material surface to the curvature plane of the first pipe bend at short mixing times. The highest stretching rate was obtained when the material surface was initially perpendicular to the symmetry plane of the first pair of Dean vortices. These findings agree well with the results of other mixing studies available in the subject literature. The effect of the initial orientation of the material surface at the mixer inlet on the energetic efficiency of mixing is present for both short and long mixing times. Besides, the long-time values of time-averaged energetic efficiency of mixing show the global maximum for Re $\cong$ 700 close to 0.1. Calculations of the flow average energetic efficiency of mixing also demonstrated the global maximum for Re $\cong$ 600 close to 0.08. Finally, it was found that the size of the unmixed fluid lumps could be decreased by almost eight orders of magnitude in the twisted bend mixer for Re $\geq$ 1000.

The present work showed that the quantification of mixing in terms of the stretching rate of the material surface and the energetic efficiency of mixing offers valuable insight into mixing processes and allows to identify optimum operating conditions for the tube mixers of curved geometry.

SYMBOLS

A	area of the material surface, m^2
a_V	concentration of material surface area, 1/m
C_f	Fanning friction factor
$\overline{\overline{D}}$	the rate of deformation tensor, 1/s
d	channel diameter, m
$\mathrm{d}\vec{A}$	differential surface, m^2
$\mathrm{d}\vec{l}$	differential material line, m
$\mathrm{d}V$	differential material volume, m^3
E	residence time distribution function
eff	energetic efficiency of mixing
l	length of material line, m
$\vec{n}$	unit direction vector
p	pressure, Pa
R	channel radius, m
R_c	channel curvature, m
Re	Reynolds number
S	channel cross-section, m^2
t	time, s
$\bar{t}$	mean residence time, s
$\vec{v}$	fluid velocity, m/s
$\bar{v}$	mean flow velocity at channel cross-section, m/s
v_x, v_y	transverse velocity components, m/s

v_z axial velocity component, m/s
$\vec{X}^+$ fluid motion, m
$\vec{x}$ coordinate vector, m

Greek symbols

α the stretching rate of surface area, 1/s
α_j the rate of linear strain, 1/s
δ channel curvature
ε dissipation rate of mechanical energy, kg/(m·s^3)
ϕ the initial inclination of the material surface, degrees
$\dot{\gamma}$ shear rate, 1/s
η area stretch
μ dynamic viscosity, kg/(m·s)
θ rate of volumetric strain, 1/s
ρ density, kg/m^3
τ dimensionless residence time

Subscripts

A refers to a finite material surface
P refers to a material point
0 initial value
1 mixer inlet
2 mixer outlet

Operators

∇ nabla
$\langle\ \rangle$ time average
$\langle\langle\ \rangle\rangle$ flow average

ACKNOWLEDGEMENTS

The Warsaw University of Technology has funded this work, project I-Chem. 1 granted by the Council of Scientific Discipline “Chemical Engineering”.

REFERENCES

Aref H., 1984. Stirring by chaotic advection. *J. Fluid Mech.*, 143, 1–21. DOI: 10.1017/S0022112084001233.

Aris R., 1989. *Vectors, tensors and the basic equations of fluid mechanics*. Dover Publications, Inc., New York.

Bałdyga J., Rożeń A., Mostert F., 1998. A model of laminar micromixing with application to parallel chemical reactions. *Chem. Eng. J.*, 69, 7–20. DOI: 10.1016/S1385-8947(97)00101-0.

Boesinger C., Le Guer Y., Mory M., 2005. Experimental study of reactive chaotic flows in tubular reactors. *AIChE J.*, 51, 2122–2132. DOI: 10.1002/aic.10455.

Castelain C., Berger D., Legentilhomme P., Mokrani A., Peerhossaini H., 2000. Experimental and numerical characterisation of mixing in a steady spatially chaotic flow by means of residence time distribution measurements. *Int. J. Heat Mass Transfer*, 43, 3687–3700. DOI: 10.1016/S0017-9310(99)00363-4.

Dean W.R., 1928. The stream-line motion of fluid in a curved pipe. *Philos. Mag. J. Sci.*, 5, 673–695. DOI: 10.1080/14786440408564513.

Heniche M., Tanguy P.A., Reeder M.F., Fasano J.B., 2005. Numerical investigation of blade shape in static mixing. *AIChE J.*, 51, 44–58. DOI: 10.1002/aic.10341.

Jones S.W., Thomas O.M., Aref H., 1989. Chaotic advection by laminar flow in a twisted pipe. *J. Fluid. Mech.*, 209, 335–357. DOI: 10.1017/S0022112089003137.

Khot P., Mansour M., Thevenin D., Nigam K. D. P., Zahringer K., 2019. Improving the mixing characteristics of coiled configurations by early flow inversion. *Chem. Eng. Res. Des.*, 146, 324–335. DOI: 10.1016/j.cherd.2019.04.016.

Kováts P., Velten C. Mansour M. Thévenin D., Zähringer K., 2020. Mixing characterisation in different helically coiled configurations by laser-induced fluorescence. *Exp. Fluids*, 61, 203. DOI: 10.1007/s00348-020-03035-0.

Kumar V., Aggarwal M., Nigam K.D.P., 2006. Mixing in curved tubes. *Chem. Eng. Sci.*, 61, 5742–5753. DOI: 10.1016/j.ces.2006.04.040.

Liang D., Zhang S., 2014. A contraction-expansion helical mixer in the laminar regime. *Chin. J. Chem. Eng.*, 22, 261–266. DOI: 10.1016/S1004-9541(14)60035-5.

Manlapaz R.L., Churchill S.W., 1981. Fully developed laminar convection from a helical coil. *Chem. Eng. Commun.*, 9, 185–200. DOI: 10.1080/00986448108911023.

Mansour M., Koth P., Kováts P., Thévenin D., Zähringer K., Janiga G., 2020a. Impact of computational domain discretisation and gradient limiters on CFD results concerning liquid mixing in a helical pipe. *Chem. Eng. J.*, 383, 123121. DOI: 10.1016/j.cej.2019.123121.

Mansour M., Liu Z., Janiga G., Nigam K. D. P., Sundmacher K., Thevenin D., Zahringer K., 2017. Numerical study of liquid-liquid mixing in helical pipes. *Chem. Eng. Sci.*, 172, 250–261. DOI: 10.1016/j.ces.2017.06.015.

Mansour M., Thevenin D., Zahringer K., 2020b. Numerical study of flow mixing and heat transfer in helical pipes, coiled flow inverters and a novel coiled configuration. *Chem. Eng. Sci.*, 221, 115690. DOI: 10.1016/j.ces.2020.115690.

Mitrinović D.S., Pečarić J.E., Fink A.M., 1993. *Classical and new inequalities in analysis*. Kluwert Academic Publishers, Dodrecht.

Moulin P., Serra C., Rouch J.C., Clifton M.J., Aptel P., 1996. Mass transfer improvement by secondary flows: Dean vortices in coiled tubular membranes. *J. Membr. Sci.*, 114, 235–244. DOI: 10.1016/0376-7388(95)00323-1.

Mridha M., Aggarwal P., Nigam K.D.P., 2011. Liquid-liquid mixing in coiled flow inverter. *Ind. Eng. Chem. Res.*, 50, 13230–13235. DOI: 10.1021/ie2002473.

Nandakumar K., Masliayh J.H., 1982. Bifurcation in steady laminar flow through curved tubes. *J. Fluid Mech.*, 119, 475–490. DOI: 10.1017/S002211208200144X.

Ottino J.M., Ranz W.E., Macosko C.W., 1979. A lamellar model for analysis of liquid-liquid mixing. *Chem. Eng. Sci.*, 34, 877–890. DOI: 10.1016/0009-2509(79)85145-3.

Palmer K.J., 2009. Shadowing lemma for flows. *Scholarpedia*, 4, 7918. DOI: 10.4249/scholarpedia.7918.

Rożeń A., 2008. Mikromieszanie płynów różniących się lepkością w układach z przepływem laminarnym. *Prace Wydziału Inżynierii Chemicznej i Procesowej PW*, XXXII (z. 1), Oficyna Wydawnicza PW.

Rożeń A., Kopytowski J., 2018. Application of the reactive tracer method to study chaotic mixing in a twisted bend mixer. *Inż. Ap. Chem.*, 57, 3, 77–78.

Rożeń A., Kopytowski J., 2020. Experimental study of micromixing in curved tube reactors by the reactive tracer method. *Chem. Eng. Res. Des.*, 160, 335–350. DOI: 10.1016/j.cherd.2020.04.042.

Sawyers D.R., Sen M., Chang H.-C., 1996. Effect of chaotic interfacial stretching on bimolecular chemical reaction in helical-coil reactors. *Chem. Eng. J.*, 64, 129–139. DOI: 10.1016/S0923-0467(96)03132-6.

Saxena A.K., Nigam K.P.D., 1983. Laminar dispersion in helically coiled tubes of square cross section. *Can. J. Chem. Eng.*, 61, 53–57. DOI: 10.1002/cjce.5450610109.

Schuler J., Herath J., Kockmann N., 2021. 3D investigations of microscale mixing in helically coiled capillaries. *J. Flow Chem.*, 11, 217–222. DOI: 10.1007/s41981-021-00161-6.

Souvaliotis A., Jana S.C., Ottino J.M., 1995. Potentialities and limitations of mixing simulations. *AIChE J.*, 41, 1605–1621. DOI: 10.1002/aic.690410702.

Vashisth S., Kumar V., Nigam K.D.P., 2008. A review on the potential applications of curved geometries in process industry. *Ind. Eng. Chem. Res.*, 47, 3291–3371. DOI: 10.1021/ie701760h.

Verma V., Topalovic A., Monechi G., Asludani A., Nigam K.D.P., 2020. Mixing of viscoelastic fluid flows in a coiled flow inverter. *Ind. Eng. Chem. Res.*, 59, 3854–3864. DOI: 10.1021/acs.iecr.9b05142.

Yamagishi A., Inaba T., Yamaguchi Y., 2007. Chaotic analysis of mixing enhancement in steady laminar flows through multiple pipe bends. *Int. J. Heat Mass Transfer*, 50, 1238–1247. DOI: 10.1016/j.ijheatmasstransfer.2006.09.033.

Received 17 August 2021
Received in revised form 22 October 2021
Accepted 25 October 2021